ICASE

ITERATIVE SPECTRAL METHODS AND SPECTRAL SOLUTIONS TO COMPRESSIBLE FLOWS

M. Yousuff Hussaini

Thomas A. Zang

Report No. 82-40

November 30, 1982

INSTITUTE FOR COMPUTER APPLICATIONS IN SCIENCE AND ENGINEERING
NASA Langley Research Center, Hampton, Virginia 23665

Operated by the

UNIVERSITIES SPACE USRA RESEARCH ASSOCIATION

ITERATIVE SPECTRAL METHODS AND SPECTRAL SOLUTIONS TO COMPRESSIBLE FLOWS

M. Y. Hussaini
Institute for Computer Applications in Science and Enginering

T. A. Zang
College of William and Mary

ABSTRACT

A spectral multi-grid scheme is described which can solve pseudospectral discretizations of self-adjoint elliptic problems in O(N log N) operations. An iterative technique for efficiently implementing semi-implicit time-stepping for pseudospectral discretizations of Navier-Stokes equations is discussed. This approach can handle variable coefficient terms in an effective manner. Pseudospectral solutions of compressible flow problems are presented. These include one-dimensional problems and two-dimensional Euler solutions. Results are given both for shock-capturing approaches and for shock-fitting ones.

Work was supported by the National Aeronautics and Space Administration under NASA Contracts No. NAS1-15810 and NAS1-16394 for the first author while he was in residence at ICASE, NASA Langley Research Center, Hampton, VA. 23665. Research was supported under NASA Grant NAG1-109 for the second author.

INTRODUCTION

Spectral methods have clear advantages provided that the discrete spectral equations can be solved efficiently and that the solution to the continuous problem is well-behaved ([1], [2]). Efficient direct solutions of spectral equations are generally possible only for simple geometries and with explicit spectral equations, although a few constant coefficient cases can be solved cheaply by direct methods. In other circumstances iterative methods are necessary. The key approach of approximating the full spectral operator with a sparse finite difference one was developed by Orszag [3] and by Morchoisne [4]. The first half of this paper will describe some recent progress on iterative schemes for elliptic problems and on iterative solutions of semi-implicit, time-stepping procedures for Navier Stokes equations. The second part of the paper will describe some recent progress that has been made on the application of spectral methods to compressible flow problems with shock waves.

2. SPECTRAL MULTI-GRID METHODS

The self-adjoint elliptic equation

$$-\nabla\cdot(a\nabla u) = f, \tag{2.1}$$

where $u(\underline{x})$ is the solution, $f(\underline{x})$ the forcing and $a(\underline{x})$ the variable coefficient, arises in many contexts. In two or more dimensions direct "fast Poisson solvers" [5] are not applicable, even for the simplest discretizations and geometries. Perhaps the most efficient iterative schemes for finite difference and finite element discretizations of these problems employ multi-

grid techniques ([6] - [8]). Theoretical estimates indicate that satisfactory convergence can be achieved in $O(N)$ arithmetic operations, where N is the total number of grid points. Zang, Wong, and Hussaini [9] have recently devised effective multi-grid procedures for the solution of pseudo-spectral discretizations of equation (2.1). A summary of that work follows along with some new developments.

For simplicity and clarity, the one-dimensional version of equation (2.1) with periodic boundary conditions on $[0,2\pi]$ will be used to explain the spectral multi-grid (SMG) approach. Write the Fourier pseudospectral discretization using N collocation, or grid, points as

$$LV = F \tag{2.2}$$

in obvious notation. Consider first a standard single-grid scheme employing Richardson relaxation

$$v \leftarrow v + \omega(F - Lv), \tag{2.3}$$

where v is the latest approximation to V and ω is a relaxation parameter. Label the real and positive eigenvalues of L as $\lambda_1,\lambda_2,\cdots,\lambda_N$ in order of increasing magnitude. The error at any stage, $v - V$, can be resolved into an expansion in the eigenvectors of L. Each iteration reduces the error component corresponding to λ_j to $\nu(\lambda_j)$ times its previous value, where

$$\nu(\lambda) = 1 - \omega\lambda. \tag{2.4}$$

The optimal choice of ω results from minimizing $|\nu(\lambda)|$ for $\lambda \in [\lambda_1,\lambda_N]$. This produces an optimal single-grid spectral radius

(2.5) $$\rho = (\lambda_N - \lambda_1)/(\lambda_N + \lambda_1).$$

The efficiency of this single-grid approach is evident in the constant coefficient case $a(x) = 1$. The eigenvalues $\lambda_j = \lfloor (j/2) \rfloor^2$ and thus $\rho \cong 1 - 8/N^2$. (The fact that $\lambda_1 = 0$ is associated with the non-uniqueness of this special problem. One should really use λ_2 in place of λ_1 in equation (2.5) for this case.) This implies that $O(N^2)$ iterations are required to achieve convergence. Combined with the $O(N \log N)$ cost per iteration (due to the spectral evaluation of Lv) this produces a total cost of $O(N^3 \log N)$.

The spectral multi-grid approach can obtain the solution in $O(N \log N)$ operations since the number of iterations turns out to be independent of N. This is explained in what follows. Define a series of grids (or levels) for $k = 2,3,\cdots,K$, each consisting of N_k uniformly spaced points, where $N_k = 2^k$. The solution to equation (2.2) is obtained by combining Richardson iterations on level K with Richardson iterations for related problems on the coarser levels $k < K$. Denote the relevant discrete problem at any level k by

(2.6) $$L_k V_k = F_k.$$

On the finest level K, $L_K = L$, $F_K = F$ and the solution $V_K = V$, the solution to equation (2.2). At any stage in the iterative solution process for equation (2.6), only an approximation v_k to the exact answer V_k is available. If this approximation is deemed adequate, then the approximation on the next-finer level $k+1$ is corrected via

(2.7) $$v_{k+1} \leftarrow v_{k+1} + P_{k+1} v_k.$$

The matrix P_k represents the coarse-to-fine interpolation of corrections from level $k-1$ to level k. On the other hand, if the approximation v_k is deemed inadequate, either another relaxation is performed, via

$$v_k \leftarrow v_k + \omega_k(F_k - L_k v_k), \tag{2.8}$$

or else control shifts to a problem on the next-coarser level $k-1$. The relaxation parameter ω_k on level k is chosen to damp preferentially those error components which are not represented on coarser grids. The right-hand-side of the coarser grid problem is obtained from

$$F_{k-1} = R_k(F_k - L_k v_k). \tag{2.9}$$

The matrix R_k represents the fine-to-coarse residual transfer from level k to level $k-1$.

The natural interpolation operators in the present context represent trigonometric interpolation. They have the useful property that R_k is the adjoint of P_k. Numerous multi-grid investigations have determined that it is desirable for the coarse grid discretization operators to satisfy

$$L_{k-1} = R_k L_k P_k. \tag{2.10}$$

This is easily implemented by modifying the usual pseudo-spectral computation of $(av_x)_x$. On the finest level $k = K$ the pointwise values of $a(x)$ are retained but on the coarser levels $\tilde{a}(x)$ is used instead, where $\tilde{a}(x)$ is obtained via trigonometric interpolation on the square roots of the finest grid values of $a(x)$. This filtering of the coefficients may be viewed as a

de-aliasing procedure. Further details on the interpolation operators are given in [9].

An essential part of any multi-grid algorithm is a specific control structure that determines when attention is shifted from one grid to another. See [7] for some flow charts and [10] for additional variations and assessments.

To appreciate why the number of iterations is independent of $N = N_K$, consider the eigenvalues of the constant coefficient case. The objective of the relaxation scheme on level K is to minimize $|\nu(\lambda)|$ only for $\lambda \in [(1/16)N^2, (1/4)N^2]$. The upper bound on $|\nu(\lambda)|$ for this minimax problem is called the smoothing rate and is denoted by μ. A simple calculation reveals that $\mu = 3/5$. This is substantially less than 1 and, perhaps more importantly, it is independent of N. A similar result obtains for the two-dimensional version as indicated in Table 1 for several $n \times n$ grids. Of course, the work on the coarser levels $k < K$ should also be counted. The relaxations there are much cheaper and the same smoothing rate applies. A more subtle issue is whether the various interpolations magnify some error components. The numerical results in [9] suggest that this effect is relatively insignificant.

Table 1. Convergence Rates for Fourier Richardson Iteration in Two-dimensions

n	Single-grid Spectral Radius	Multi-grid Smoothing Rate
4	0.333	0.333
8	0.895	0.636
16	0.980	0.719
32	0.996	0.751
64	0.999	0.765
∞	1.000	0.778

When Dirichlet boundary conditions are applied to equation (2.1), Chebyshev polynomials are more appropriate than Fourier series. The additional complication here is that $\lambda_N = O(N^4)$ whereas $\lambda_{N/2} = O(N^2)$. The ratio of these two numbers determines the smoothing rate. (This ratio may be termed the multi-grid condition number.) Since this multi-grid condition number grows dramatically with N, the straightforward use of Richardson iteration leads to a smoothing rate which tends rapidly to 1.

The cure is to pre-condition the iteration by applying

$$v \leftarrow v + \omega H^{-1}(F-Lv), \tag{2.11}$$

where H is some readily-invertible approximation to L. An obvious choice for H is a finite difference approximation H_{FD} to equation (2.1) as proposed in [3] and [4] for single-grid iterations. However, in more than one-dimension these finite difference approximations are themselves costly to invert. A more desirable choice is an approximate LU-decomposition of H_{FD}, i.e., H is taken as the product of a lower triangular matrix L and an upper triangular matrix U. In one such type of preconditioning, denoted by H_{LU}, L is identical to the lower triangular portion of H_{FD} and U is chosen so that the two super diagonals of LU agree with those of H_{FD}. In [9] an alternative pre-conditioning, denoted here by H_{RS}, was proposed in which the diagonal elements of L were altered from those of H_{FD} to ensure that the row sums of H_{RS} and H_{FD} were identical.

The essential properties of all three types of pre-conditioning are shown in Table 2 for the constant coefficient problem. The total number of grid points $N = n^2$. The eigenvalues shown there were computed numerically. In order to assess the effectiveness of these pre-conditionings in multi-grid

Table 2. Extreme Eigenvalues for Pre-conditioned Chebyshev Operator in Two-dimensions

n	$H_{FD}^{-1}L$		$H_{LU}^{-1}L$		$H_{RS}^{-1}L$	
	λ_{min}	λ_{max}	λ_{min}	λ_{max}	λ_{min}	λ_{max}
4	1.000	1.757	0.929	1.717	1.037	1.781
8	1.000	2.131	0.582	2.273	1.061	2.877
16	1.000	2.305	0.224	2.603	1.043	4.241
24	1.000	2.361	0.111	2.737	1.031	5.379

calculations, one also needs to know the smallest "high frequency" eigenvalue. The numerical results indicate that this is 1.22 for H_{FD} and H_{LU} and 1.45 for H_{RS}, essentially independent of n. The relevant condition numbers are given in Table 3. Both H_{LU} and H_{RS} require only O(N) operations to invert. Thus, we reach the striking conclusion that although H_{RS} is more effective for single-grid iterations, H_{LU} is noticeably superior in the multi-grid context. Moreover, H_{FD} offers little improvement in smoothing rate over H_{LU}. Since H_{FD} is much costlier to invert, H_{LU} is the preferred multi-grid pre-conditioning. Table 4 indicates the convergence rates which can be obtained with the approximate LU-decomposition. Numerical evidence suggests an upper bound of 0.4 for the multi-grid smoothing rate.

The tables in this section indicate the theoretical performance of SMG on constant coefficient problems. The numerical calculations reported in [9] confirm that these convergence rates are achieved in practice, even for variable coefficient problems. Recent calculations for the H_{LU} pre-conditioning confirm that it, too, behaves as predicted [11].

Table 3. Condition Number for Pre-conditioned Chebyshev Operator in Two-dimensions

n	Single-grid		Multi-grid	
	$H_{LU}^{-1}L$	$H_{RS}^{-1}L$	$H_{LU}^{-1}L$	$H_{RS}^{-1}L$
4	1.85	1.72		
8	3.91	2.71	1.79	2.07
16	11.62	4.07	2.12	2.92
24	24.66	5.22	2.26	3.79

Table 4. Convergence Rates for Chebyshev Richardson Iteration in Two-dimensions

n	Single-grid Spectral radius	Multi-grid Smoothing Rate
4	0.264	0.298
8	0.462	0.283
16	0.605	0.358
24	0.678	0.387

Spectral multi-grid methods can certainly be applied to a wider set of problems than covered by equation (2.1) with periodic or Dirichlet boundary conditions. Effective methods exist for other boundary conditions, such as Dirichlet in one direction and periodic in the other. Non-self-adjoint and nonlinear problems, including systems of equations, can also be handled. Results for single grid calculations will be presented elsewhere ([12]).

3. SEMI-IMPLICIT TIME-STEPPING METHODS FOR NAVIER-STOKES EQUATIONS

An important source of implicit variable coefficient spectral equations is semi-implicit time-stepping algorithms for evolution equations with spectral spatial discretizations. Efficient iterative schemes are especially needed for Chebyshev spectral methods due to their severe explicit time-step limitations and the expense of direct solutions of the implicit equations in all but the simplest cases.

The incompressible Navier-Stokes equations are an important application. The rotation form equations for two-dimensional channel flow are

$$u_t - v(v_x - u_y) + P_x = (\mu u_x)_x + (\mu u_y)_y \tag{3.1}$$

$$v_t + u(v_x - u_y) + P_y = (\mu v_x)_x + (\mu v_y)_y \tag{3.2}$$

$$u_x + v_y = 0, \tag{3.3}$$

with periodic boundary conditions in x and no-slip boundary conditions at $y = \pm 1$. The variable P denotes the total pressure. The viscosity μ is presumed to depend upon y.

A useful discretization employs Fourier series in x and Chebyshev series in y. The pressure gradient term and the incompressibility constraint are best handled implicitly. So, too, are the vertical diffusion terms because of the fine mesh-spacing near the wall. The variable viscosity prevents the standard Poisson equation for the pressure from decoupling from the velocities in the diffusion term. The algorithm described in [13] appears to be a good starting point. A Crank-Nicolson approach is used for the implicit terms and Adams-Bashforth for the remainder. After a Fourier transform in x, the equations for each wavenumber k have the following implicit structure

$$\hat{u} - \tfrac{1}{2}\Delta t(\mu \hat{u}_y)_y + \tfrac{1}{2}\Delta t ik\hat{P} = \cdots \tag{3.4}$$

$$\hat{v} - \tfrac{1}{2}\Delta t(\mu \hat{v}_y)_y + \tfrac{1}{2}\Delta t\hat{P}_y = \cdots \tag{3.5}$$

$$ik\hat{u} + \hat{v}_y = 0. \tag{3.6}$$

Fourier transformed variables are denoted by hats, the subscript y denotes a Chebyshev pseudospectral derivative, and Δt is the time increment.

The algorithm in [13] was devised for constant viscosity, in which case the equations (3.4) - (3.6) can be reduced to essentially a block-tridiagonal form. This cannot be done in the present, more general situation. We advocate solving these equations iteratively after applying a finite difference pre-conditioning.

The interesting physical problems have high Reynolds number, i.e., low viscosity. Thus the first derivative terms in equations (3.4) - (3.6) predominate. The effective pre-conditioning of them is crucial. Four possibilities have been considered. The eigenvalues of pre-conditioned iterations for the model scalar problem $u_x = f$ with periodic boundary conditions on $[0,2\pi]$ are given for each possibility in Table 5. The term $\alpha\Delta x$ is the product of a wavenumber α and the grid spacing Δx. It falls in the range $0 \leq |\alpha\Delta x| \leq \pi$. For the staggered grid case the discrete equations (3.4) - (3.6) are modified so that the velocities and the momentum equations are defined at the cell faces $y_j = \cos(\pi j/N)$, $j=0,1,\cdots,N$, whereas the pressure and the continuity equation are defined at the cell centers $y_{j-1/2} = \cos(\pi(j-1/2)/N)$, $j=1,\cdots,N$. Fast cosine transforms enable interpolation between cell faces and cell centers to be implemented efficiently. The staggered grid for the Navier-Stokes equations has the advantage that no artificial boundary condition is required for the pressure at the walls.

The actual eigenvalues for pre-conditioned iterations of equations (3.4) - (3.6) are displayed in Figures 1 and 2. The model problem estimates the eigenvalue trends surprisingly well considering that it is just a scalar equation, has only first derivative terms and uses Fourier series rather than Chebyshev polynomials.

Table 5. Pre-conditioned Eigenvalues for One-dimensional First Derivative Model Problem

Pre-conditioning	Eigenvalues
Central Differences	$\frac{\alpha\Delta x}{\sin(\alpha\Delta x)}$
One-sided Differences	$e^{-i(\alpha\Delta x/2)} \frac{\alpha\Delta x/2}{\sin((\alpha\Delta x)/2)}$
High Mode Cut-off	$\begin{cases} \frac{\alpha\Delta x}{\sin(\alpha\Delta x)} & 0 < \lvert\alpha\Delta x\rvert \leq (2\pi/3) \\ 0 & (2\pi/3) < \lvert\alpha\Delta x\rvert \leq \pi \end{cases}$
Staggered Grid	$\frac{(\alpha\Delta x)/2}{\sin((\alpha\Delta x)/2)}$

The preceding results indicate that the staggered grid leads to the most effective treatment of the first derivative terms. The condition number of the pre-conditioned system is reasonably small and no resolution is lost by a high mode cut-off. (Although it is possible to devise a high-mode cut-off which avoids the small eigenvalues shown in the figures, some of the spectral resolution is thereby lost.) A simple and effective iterative scheme for this system with its complex eigenvalues is a minimum residual method. At a Reynolds number of 7500 each iteration reduces the residual by almost an order of magnitude.

This semi-implicit technique has several obvious extensions. It is easily applied to incompressible flow over a flat plate in the context of the parallel flow assumption. Pre-conditioned eigenvalues for this situation are shown in Figure 3. A substantial increase in the allowable time-steps can be achieved by treating the mean streamwise advection term in a semi-implicit fashion. This is easily implemented. Adding a third dimension with periodic

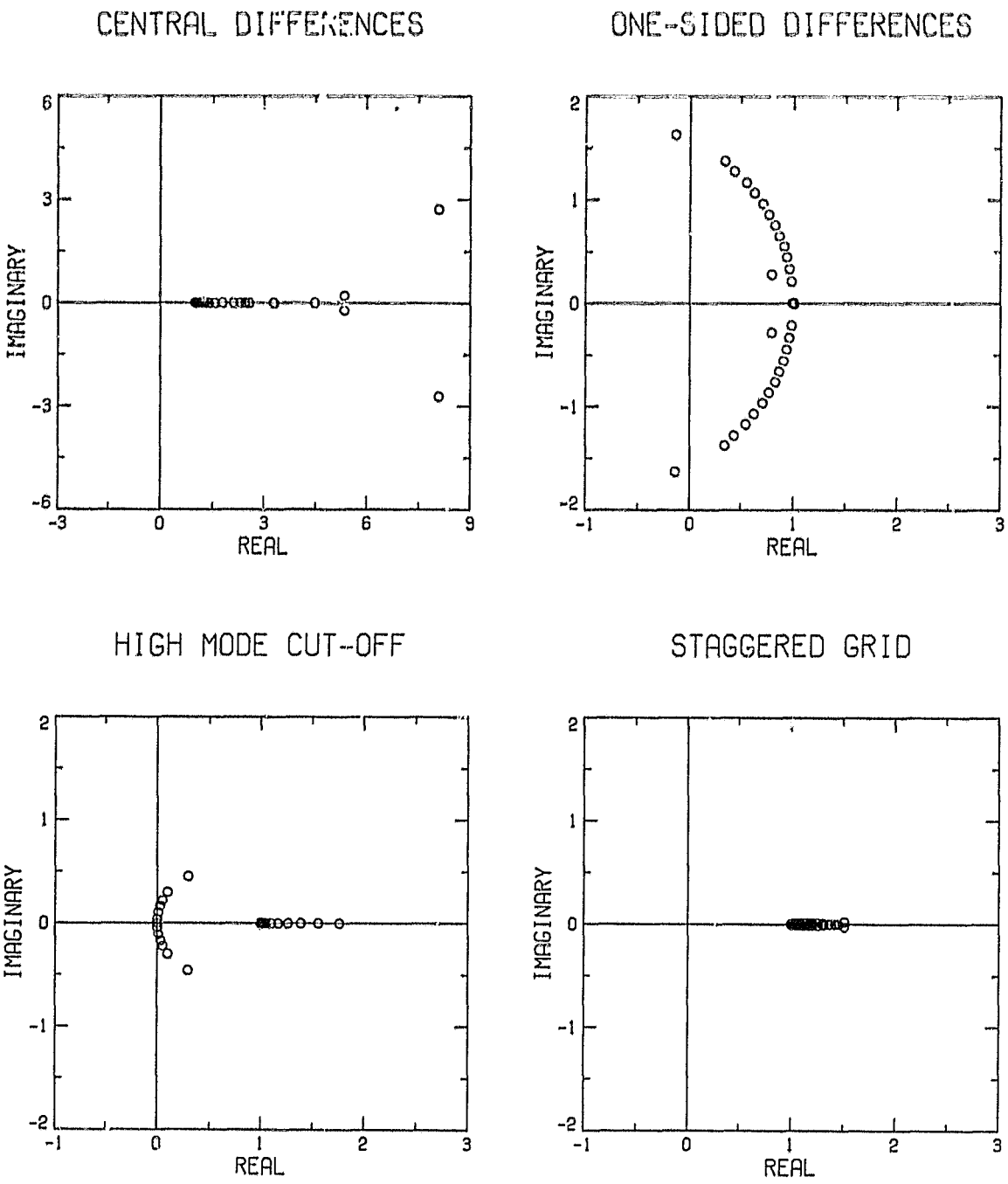

Figure 1. Eigenvalues of the pre-conditioned matrices for semi-implicit channel flow when the streamwise wave number $k = 1$. The grid is 32×17, the Reynolds number is 7500 and the CFL number is 0.10. Note the different scale used for the central differences pre-conditioning results.

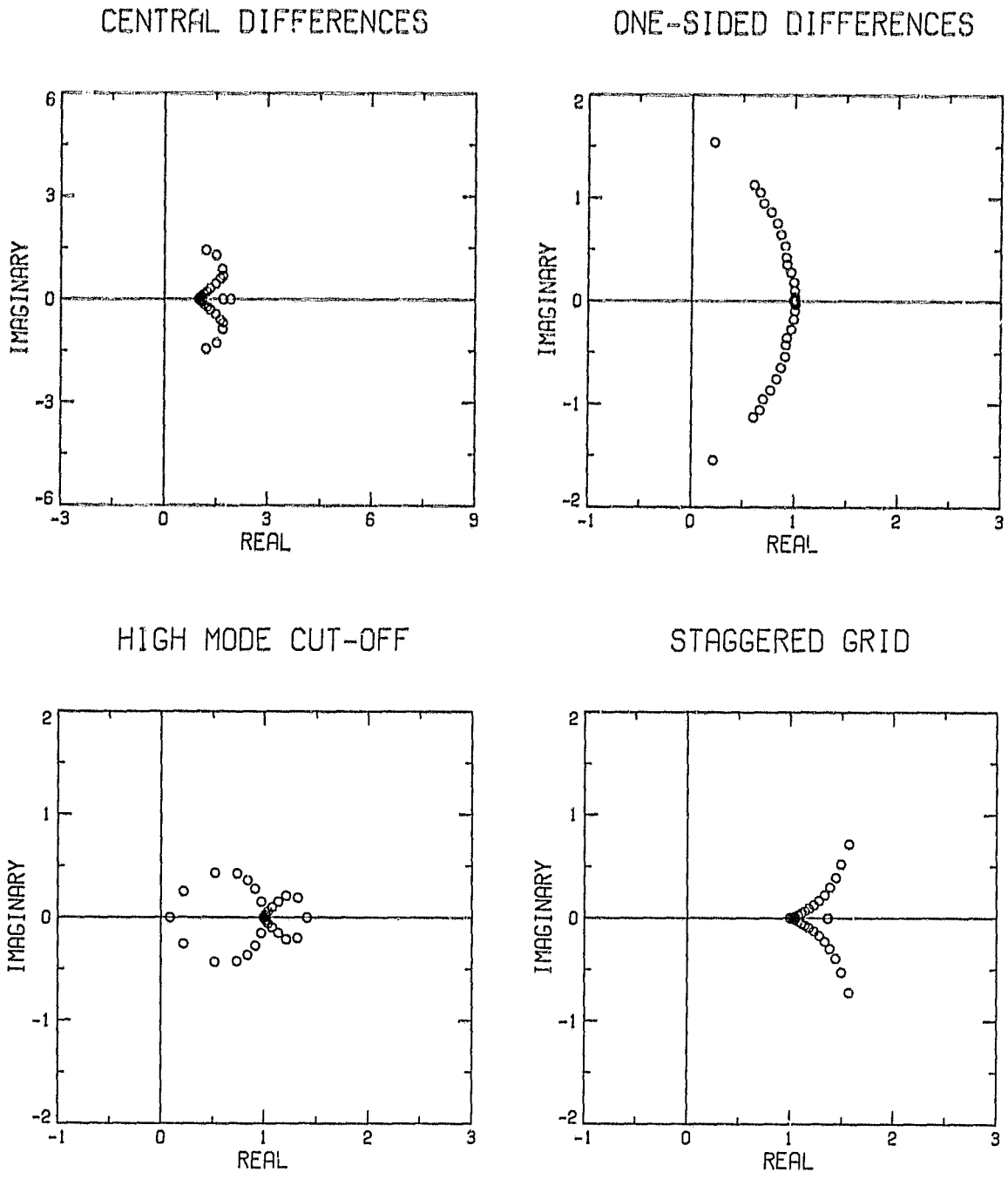

Figure 2. Eigenvalues of the pre-conditioned matrices for semi-implicit channel flow when the streamwise wave number k = 10. The grid is 32×17, the Reynolds number is 7500 and the CFL number is 0.10. Note the different scale used for the central differences pre-conditioning results.

boundary conditions is trivial, aside from storage and run-time considerations. Treating no-slip boundary conditions in two directions and/or including more of the advection terms in a semi-implicit manner is more difficult. Here, however, one can employ the approximate LU-decomposition described in section 2.

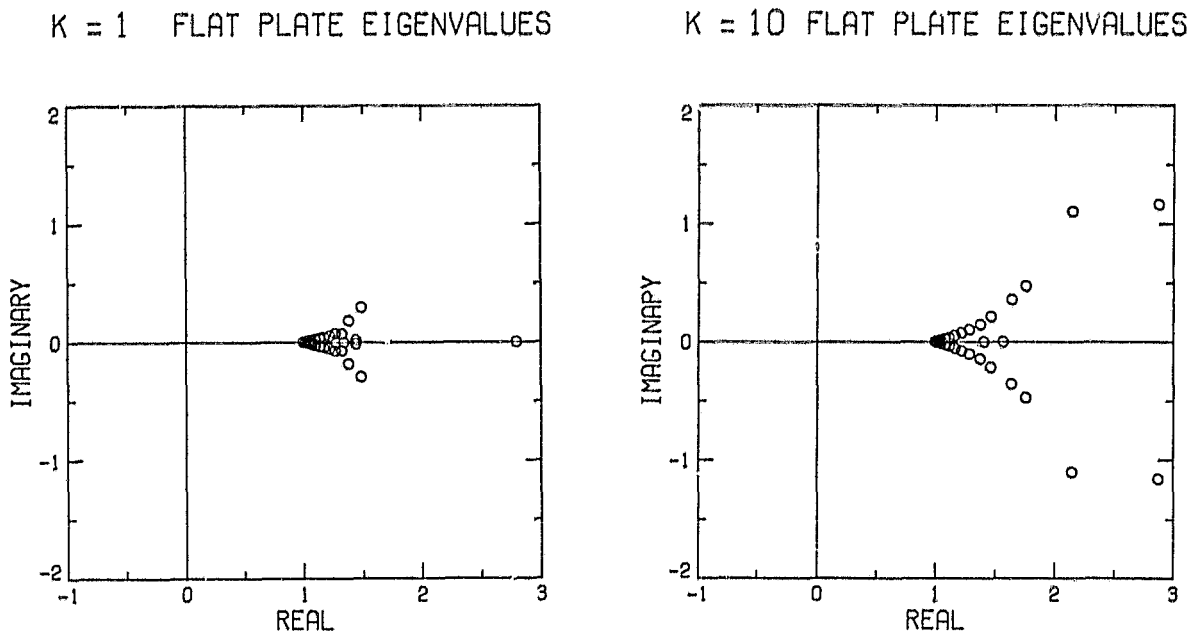

Figure 3. Eigenvalues of the staggered grid pre-conditioned matrices for semi-implicit flat plate flow. The grid is 32×17, the Reynolds number is 7500 and the CFL number is 0.10.

Further details are discussed in [14]. That report also contains numerical examples using production codes for the channel and flat plate problems in both constant viscosity and variable viscosity situations.

4. PSEUDOSPECTRAL SOLUTIONS TO COMPRESSIBLE FLOWS

4.1 Quasi-One-Dimensional Flows

Recent investigations ([15], [16],[17]) of one-dimensional problems indicate that spectral methods may provide a promising approach to compressible flows with shocks. In these calculations the shock wave is "captured" and a kind of filtering is applied to deal with the oscillations resulting from the sharp discontinuity. The goal of the filtering is to suppress the oscillations without degrading the accuracy in the smooth but structured regions of the flow. Simple flows such as those represented by piecewise linear profiles are not very demanding tests since the series representations of such functions forgive a number of filtering crimes.

Figures 4 and 5 reproduce the results presented in [15] for reasonably demanding flows. The first of these figures refers to the standard test problem of a quasi-one-dimensional nozzle flow. The second figure pertains to a rather unusual, but highly structured, astrophysical flow problem. The rapid decompression region behind the shock is especially challenging. Note that the computed shock is quite sharp and that the complex flow structure is preserved.

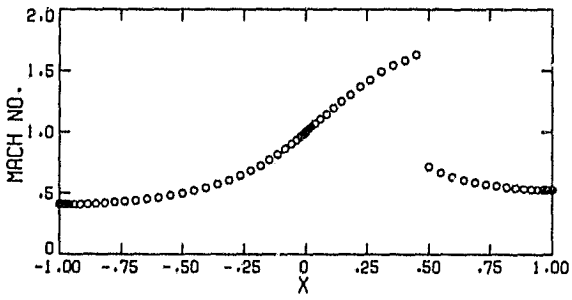

Figure 4. Chebyshev pseudo-spectral solution of transonic quasi-1-D nozzle flow.

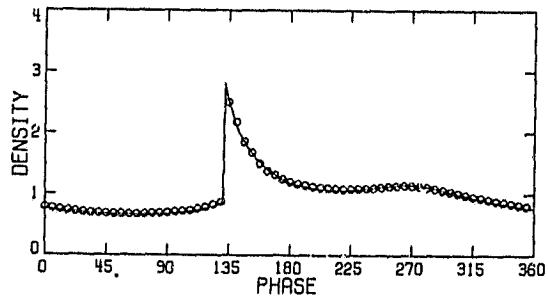

Figure 5. Fourier pseudo-spectral solution of a 1-D model of a forced galactic shock wave.

4.2 Two-Dimensional Flows

Interaction of a shock wave with an entropy spot and a vortex. The two-dimensional compressible Euler equations present a more challenging test for the spectral methods. The shock "capturing" techniques of the one-dimensional flow problems are not as successful in the two-dimensional case, and the filtering methods presently used (to deal with the Gibbs phenomena) affect the accuracy of the solution. It stands to reason that while applying pseudospectral methods to complex shock interaction problems, the spectral accuracy can be maintained by "tracking" or fitting the shock. In such cases the relevant governing equations are not necessarily cast in conservation form, and they are solved in the transformed or computational domain where the shock becomes a coordinate line. The unsteady, two-dimensional, compressible, Euler equations in the computational plane (X,Y) are written in the form,

$$Q_T + \underline{A}Q_X + \underline{B}Q_Y = 0 \tag{4.1}$$

where $Q = [P,u,v,S]^T$ and

$$\underline{A} = \begin{bmatrix} U & \gamma X_x & \gamma X_y & 0 \\ a^2 X_x/\gamma & U & 0 & 0 \\ a^2 X_y/\gamma & 0 & U & 0 \\ 0 & 0 & 0 & U \end{bmatrix} \qquad \underline{B} = \begin{bmatrix} V & \gamma Y_x & \gamma Y_y & 0 \\ a^2 Y_x/\gamma & V & 0 & 0 \\ a^2 Y_y/\gamma & 0 & V & 0 \\ 0 & 0 & 0 & V \end{bmatrix} .$$

The natural logarithm of the pressure, the speed of sound, and the entropy are represented by P, a, and S, respectively, and γ is the ratio of specific heats. The velocity in the Cartesian x and y directions are u and v, respectively. All variables are normalized with respect to reference conditions at downstream infinity, as in [18]. The contravariant velocity

components are defined by

$$U = X_t + uX_x + vX_y \quad \text{and} \quad V = Y_t + uY_x + vY_y .$$

Subscripts denote partial derivatives with respect to the independent variables.

The coordinate transformation is defined as follows:

$$X = \frac{x - h(t)}{x_s(y,t) - h(t)}$$

$$Y = \frac{\tanh(\alpha y) + 1}{2}$$

$$T = t,$$

where $x = h(t)$ is some left boundary of the interaction region and $x = x_s(y,t)$ is the shock wave front.

The computational domain is thus $(X,Y) \in [0,1] \times [0,1]$. Note the stretching (with parameter α) that has been used to handle the infinite extent of the lateral coordinate y. If the relative shock Mach number M_s is sufficiently high ($M_s > 2.08$), the flow upstream of the shock remains supersonic. In this case, the left boundary corresponds to a supersonic inflow, and all dependent variables can be prescribed on it. However, if the relative shock Mach number is low, then radiation-type boundary conditions are used at the left boundary. On the right, the computational region is bounded by the shock wave. Downstream of the shock the flow field is given analytically. The flow field immediately upstream of the shock, as well as the shape and velocity of the shock, are evaluated such that the Rankine-Hugoniot jump conditions and the compatibility condition reaching the shock wave from the upstream side are simultaneously satisfied.

Let k denote the time level and let Δt be the time step increment. The time discretization of eq. (4.1) is then as follows:

$$\tilde{Q} = [1 - \Delta t L^k] Q^k,$$

$$Q^{k+1} = 1/2\,[Q^k + (1 - \Delta t \tilde{L})\tilde{Q}],$$

where the spatial operator L represents an approximation to $\underline{A}\partial/\partial X + \underline{B}\partial/\partial Y$. In the pseudospectral method, the solution Q is first expanded as a double Chebyshev series,

$$Q(X,Y,T) = \sum_{p=0}^{M} \sum_{q=0}^{N} Q_{pq}(T)\tau_p(\xi)\tau_q(\eta),$$

where

$$\xi = 2X - 1 \quad \text{and} \quad \eta = 2Y - 1,$$

and τ_p and τ_q are the Chebyshev polynomials of degrees p and q. The derivatives appearing in the spatial operators are then evaluated as

$$Q_X = 2 \sum_{p=0}^{M} \sum_{q=0}^{N} Q_{pq}^{(1,0)} \tau_p \tau_q,$$

where

$$Q_{pq}^{(1,0)} = \frac{2}{c_p} \sum_{\substack{m=p+1 \\ m+p \text{ odd}}}^{M} m Q_{mq},$$

and

$$c_0 = 2, \quad c_p = 1, \; p > 0.$$

The evaluation of the shock wave shape and velocity followed the same procedure outlined above including spectral evaluation of the derivatives on

the upstream side of the shock are expressed as Chebyshev expansions. At the left boundary, all variables were specified for supersonic inflow. For the case of subsonic inflow, the two velocity components and the entropy were specified, while the pressure was computed from a quasi-one-dimensional characteristic.

The pseudospectral method has a tendency to develop slowly growing oscillations. Because of the global nature of this method they are spread over the entire flow field rather than being confined to the vicinity of sharp gradients. The underlying smooth solution can be recovered by a variety of filtering techniques. The results presented here were obtained by applying a von Hann window filter (see [15] for details) every 160 time steps.

Figure 6 shows a plane shock wave about to interact with a hot spot (situated in a quiescent field) with the temperature distribution σ given by

$$\sigma = k \exp\{-[(x-x_0)^2 + (y-y_0)^2]/2r^2\},$$

where $k = 0.25$, $r = 1.25$, $x_0 = 0.5$ and $y_0 = 0$. The initial shock position is $x = 0$, and its initial Mach number is 3. Figure 7 displays vorticity contours at time $t = 0.2$ when the shock wave has passed over the hot spot. See [18] for more details on the physics and [19] for comparisons with finite difference calculations.

Figure 8 shows the velocity field for a single vortex about to interact with a shock wave traveling initially with speed $M_s = 3$. The downstream conditions here are obtained by assuming a constant density field, calculating the velocity from the stream function,

$$\phi = \frac{\kappa}{2\pi} \log \sqrt{r^2 + (x-x_0)^2 + (y-y_0)^2},$$

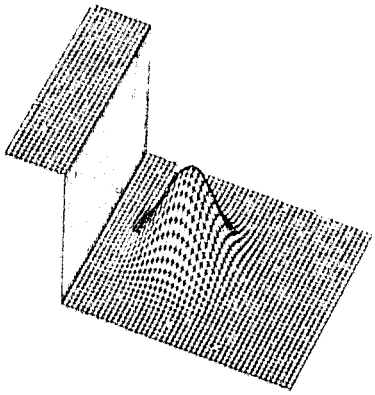

Figure 6. Surface plot of entropy for a hot spot and an initial advancing Mach 3 shock wave.

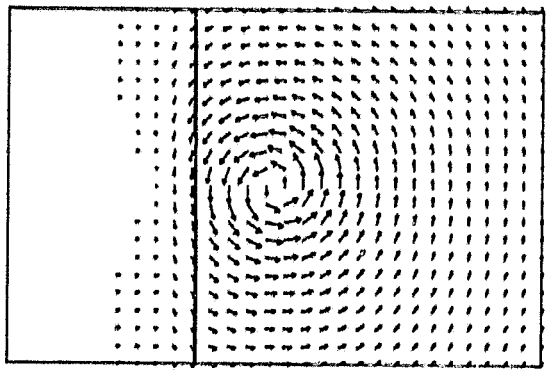

Figure 8. Velocity vectors for a vortex. Solid vertical line denotes an advancing Mach 3 shock wave.

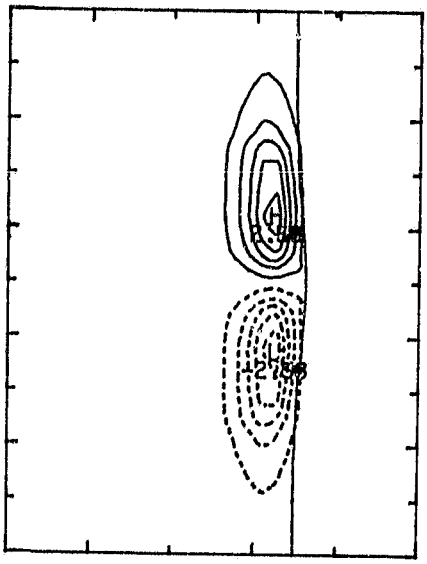

Figure 7. Vorticity contours from pseudospectral calculation for a hot spot after interaction with a Mach 3 shock wave (solid line).

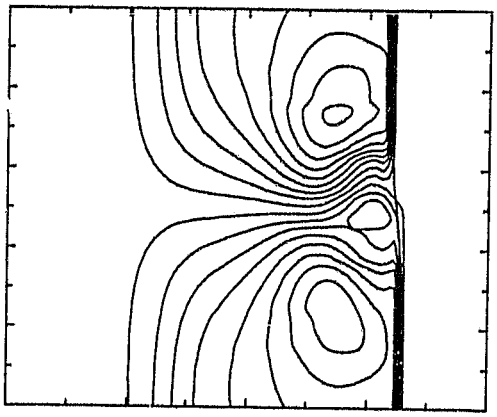

Figure 9. Pressure contours from pseudospectral calculation for a vortex after interaction with a Mach 3 shock wave.

the pressure from Bernoulli's relation, and the temperature from the equation of state. For the case shown in Figure 8, the circulation $\kappa=2$ and the softening scale $r=0.1$. This model approaches an idealized incompressible point vortex at large distances but is much smoother near the center. Figure

9 shows the resulting pressure field after the shock wave has passed over the vortex. See [20] for more details on the physics and [19] for comparisons with finite difference calculations.

Compressible Flow Past a Circular Cylinder

Blunt body problem. As pointed out in [21] the classical problem of a blunt body in a supersonic stream has been an ideal test problem for numerical methods as it provides a relatively simple well-posed transonic problem with nontrivial initial and boundary conditions. The present pseudospectral method like most common methods obtains the steady state solution as the time asymptotic solution of the unsteady Euler equations which are written in the cylindrical polar coordinate (r,θ) system. The physical domain of interest consists of the known body $r = r_b(\theta)$, the unknown shock location, $r = r_s(\theta,t)$, the axis of symmetry (the front stagnation streamline $\theta = \pi$) and the outflow boundary $\theta = \pi - \overline{\theta}_{max}$. For the purpose of shock fitting, the coordinate transformation

$$X = \frac{r - r_b(\theta)}{r_s(\theta,t) - r_b(\theta)}$$

$$Y = \frac{\pi - \theta}{\overline{\theta}_{max}}$$

is introduced so that the shock wave and the body are coordinate lines in the transformed domain. The transformed equations of motion, in the notation of the previous problem, are

$$Q_T + \underline{A}Q_X + \underline{B}Q_y + R = 0,$$

where $Q = [P,u,v,S]^T$ and

$$\underline{A} = \begin{bmatrix} U & \gamma X_r & (\gamma/r)X_\theta & 0 \\ (a^2/\gamma)X_r & U & 0 & 0 \\ (a^2/\gamma)(1/r)X_\theta & 0 & U & 0 \\ 0 & 0 & 0 & U \end{bmatrix},$$

$$\underline{B} = \begin{bmatrix} V & \gamma Y_r & (\gamma/r)Y_\theta & 0 \\ (a^2/\gamma)Y_r & V & 0 & 0 \\ (a^2/\gamma)(1/r)Y_\theta & 0 & V & 0 \\ 0 & 0 & 0 & V \end{bmatrix},$$

and

$$R = \left[\gamma \frac{u}{r}, -\frac{v^2}{r}, \frac{uv}{r}, 0\right]^T$$

with

$$U = X_r + uX_r + \frac{\gamma}{r} X_\theta$$

and

$$V = \frac{r}{r} Y_\theta .$$

The flow field variables P, u, v, and S are expanded in double Chebyshev series, and the solution technique is the same as for the previous problem.

The shock boundary $r = r_s(\theta,t)$ (i.e., $X = 1$) is computed using Rankine-Hugoniot jump conditions and the compatibility equation along the incoming characteristic from the high pressure side of the shock. At the symmetry line $\theta = \pi$ ($Y = 0$) the θ-component of velocity v is set equal to zero. On the body $r = r_b(\theta)$ (i.e., $X = 0$), the normal component of velocity, u, is zero. θ_{max} is chosen so that the outflow boundary $Y = 1$ is supersonic, and hence no boundary conditions need be imposed.

Figure 10 shows the Mach number contours and the velocity vectors for a circular cylinder in a uniform stream at $M_\infty = 4$. The results are found to

be in very good agreement with the tabulated values given in reference [22]. The coarse 8×8 mesh and the Chebyshev grid point distribution are evident in the velocity vector plot. Figure 11 displays the results for the linearly sheared free stream. This may be compared with Figure 12 where the finite difference results obtained on a 20×30 grid are shown.

Subsonic Flow Past a Circular Cylinder

In the case of a circular cylinder in the subsonic stream, it is expedient to map the infinite exterior domain onto the interior of a unit circle by the coordinate transformation

$$X = 1/r \qquad 0 \leq X \leq 1.$$

The dependent variables are then represented in terms of Chebyshev polynomials in X; Fourier representation in θ is appropriate as

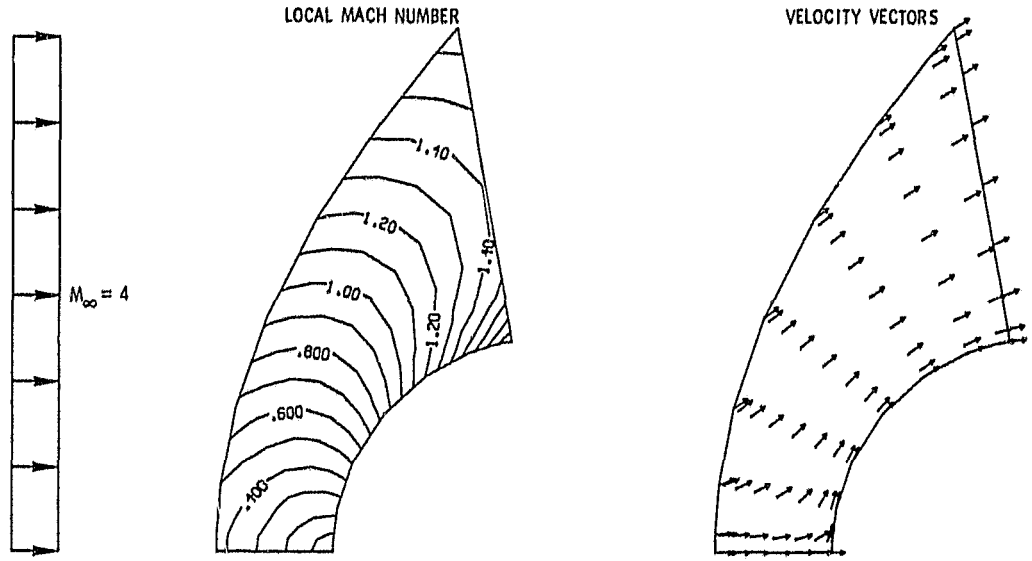

Figure 10. Pseudospectral solution on an 8×8 grid for a circular cylinder in a Mach 4 uniform stream.

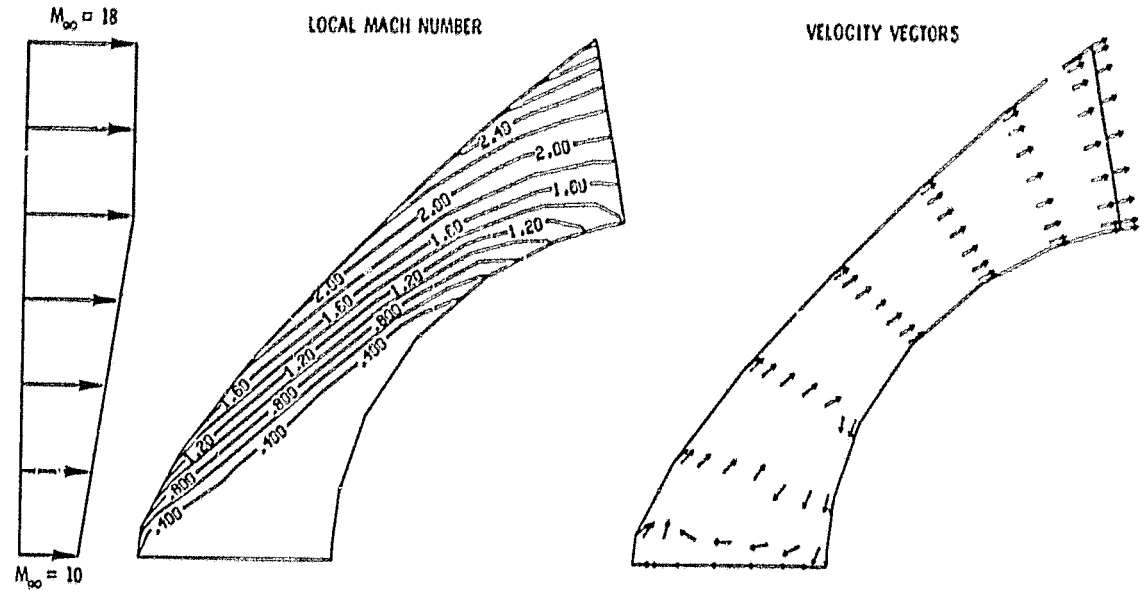

Figure 11. Pseudospectral solution on an 8×8 grid for a circular cylinder in a linearly sheared stream.

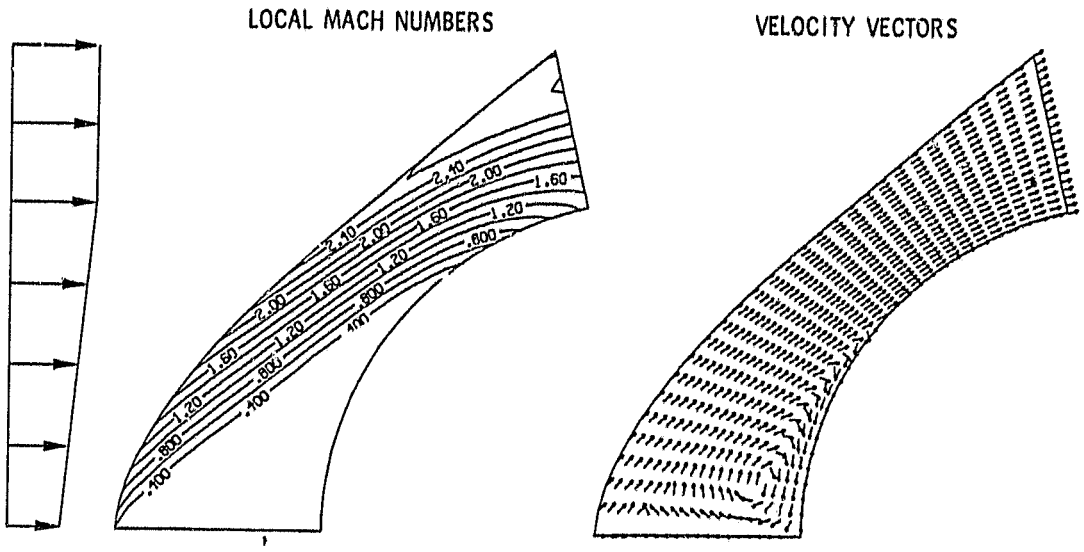

Figure 12. Finite difference solution on a 20×30 grid for a circular cylinder in a linearly sheared stream.

the flow field is periodic with period 2π. However, one needs to consider only the interval $0 \leq \theta \leq \pi$ because of symmetry. For this semi-circle problem, the dependent variables can be expanded in terms of sine and cosine functions in θ; they may again be represented by Chebyshev polynomials in θ. These two different representations are found to yield practically identical results.

Figure 13 shows the Mach number contours for the flow past a circular cylinder at $M_\infty = 0.4$ computed by a finite difference technique (120×40 mesh) and the pseudospectral method (16×8). At this free stream Mach number the incipient critical flow is attained at the top of the cylinder. The results show very good agreement between the two numerical calculations. Further comparisons, other details and additional results for various free stream Mach numbers are reported in reference [23].

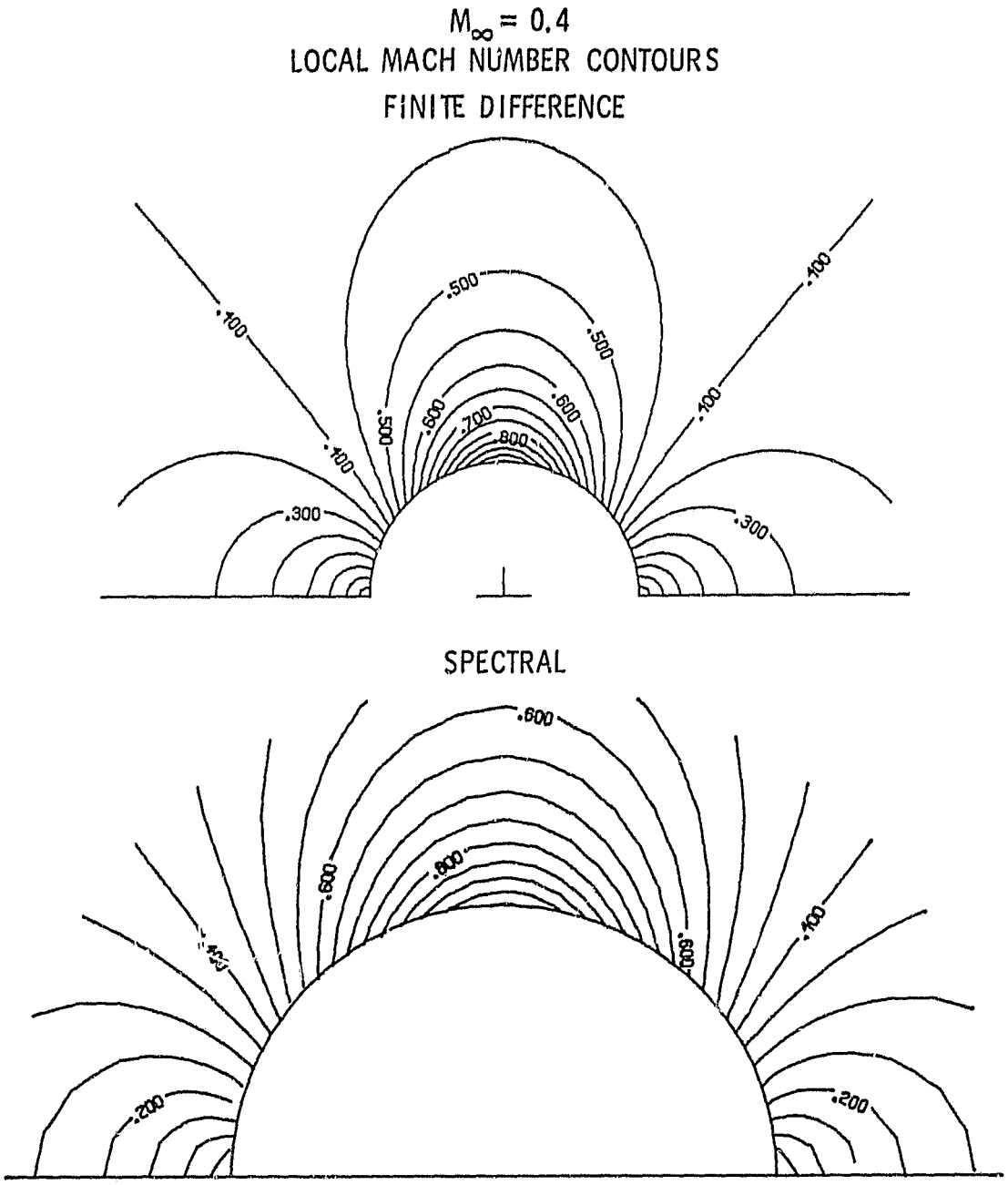

Figure 13. Finite difference and pseudospectral solutions for a circular cylinder in a Mach 0.4 uniform stream.

REFERENCES

[1] S. A. ORSZAG and M. ISRAELI, Numerical simulation of viscous incompressible flows, Ann. Rev. of Fluid Mechanics, 6, (1974), pp. 281-318.

[2] D. GOTTLIEB, and S. ORSZAG, Numerical Analysis of Spectral Methods: Theory and Applications, CBMS-NSF Regional Conference Series in Applied Mathematics, Society for Industrial and Applied Mathematics, 1977.

[3] S. A. ORSZAG, Spectral methods for problems in complex geometries, J. Comp. Phys., 37, (1980), pp. 70-92.

[4] Y. MORCHOISNE, Resolution of Navier Stokes equations by a space-time pseudo spectral method, La Recherche Aerospatial, 5, (1979), pp. 293-309.

[5] P. N. SWARTZTRAUBER, The methods of cyclic reduction, Fourier analysis and the FACR algorithm for the discrete solution of Poisson's equation on a rectangle, SIAM Rev., 19, (1977), pp. 490-501.

[6] R. P. FEDORENKO, A relaxation method for solving elliptic difference equations, Z. Vycisl. Mat. i Mat. Fix., 1, (1961), pp. 922-927.

[7] ACHI BRANDT, Multi-level adaptive solutions to boundary-value problems, Math. Comp., 31, (1977), pp. 333-390.

[8] R. A. NICOLAIDES, On multiple grid and related techniques for solving discrete elliptic systems, J. Comp. Phys., 19, (1975), pp. 418-431.

[9] T. A. ZANG, Y. S. WONG, and M. Y. HUSSAINI, Spectral multi-grid methods for elliptic equations, J. Comp. Phys., 48, (1982).

[10] H. LOMAX, editor, Multigrid Methods, NASA Conference Publication 2202, (1981).

[11] T. A. ZANG, Y. S. WONG, and M. Y. HUSSAINI, Spectral multi-grid methods for elliptic equations II,, to appear.

[12] Y. S. WONG, T. A. ZANG and M. Y. HUSSAINI, Efficient iterative solutions to spectral equations, to appear.

[13] P. MOIN and J. KIM, On the numerical solution of time-dependent viscous incompressible fluid flows involving solid boundaries, J. Comp. Physics, 35, (1980), pp. 381-392.

[14] M. R. MALIK, T. A. ZANG and M. Y. HUSSAINI, Efficient solution to semi-implicit spectral methods for Navier-Stokes equations, to appear.

[15] T. A. ZANG and M. Y. HUSSAINI, Mixed spectral-finite difference approximations for slightly viscous flows, Proc. of the 7th Intl. Conf. on Numerical Methods in Fluid Dynamics, (1981), pp. 461-466.

[16] D. GOTTLIEB, L. LUSTMAN and S. ORSZAG, Spectral calculations of one-dimensional inviscid compressible flows, SIAM J. Sci. Statis. Comput., 2, (1981), pp. 296-310.

[17] T. D. TAYLOR, R. B. MYERS and J. H. ALBERT, Pseudo-spectral calculations of shock waves, rarefaction waves and contact surfaces, Computers and Fluids, 9, (1981) pp. 469-473.

[18] T. A. ZANG, M. Y. HUSSAINI, and D. M. BUSHNELL, Numerical computations of turbulence amplification in shock wave interactions, AIAA paper 82-0293, Presented at the AIAA 20th Aerospace Sciences Meeting, January 11-13, (1982), Orlando, FL.

[19] M. D. SALAS, T. A. ZANG and M. Y. HUSSAINI, Shock-fitted Euler solutions to shock-vortex interactions, Proc. of the 8th Intl. Conf. on Numerical Methods in Fluid Dynamics, to appear.

[20] S. P. PAO and M. D. SALAS, A numerical study of two-dimensional shock vortex interaction, AIAA paper 81-1205, Presented at the AIAA 14th Fluids and Plasma Dynamics Conference, June 23-25, (1981), Palo Alto, CA.

[21] M. D. SALAS, Flow properties for a spherical body at low supersonic speeds, Presented at the Symp. on Computers in Aerodynamics, Polytechnique Institute of New York, June (1979).

[22] A. N. LYUBIMOV and V. V. RUSANOV, Gas flows past blunt bodies, (Translation of "Techeniya Gaza Okolo Tupykh Tel, Chast' II: Tablitsy Termodinamicheskikh Funktsiy," "Nauka" Press, Moscow, 1970), NASA TT F-715, February (1973).

[23] M. Y. HUSSAINI, M. D. SALAS, and T. A. ZANG, Pseudospectral solution to compressible Euler equations, to appear.